Inorg. Chem. **2002**, *41*, 5593–5601

High Nuclearity Ruthenium–Tin Clusters from the Reactions of Triphenylstannane with Pentaruthenium Carbonyl Carbido Cluster Complexes

Richard D. Adams,* Burjor Captain, Wei Fu, and Mark D. Smith

Department of Chemistry and Biochemistry and USC NanoCenter, University of South Carolina, Columbia, South Carolina 29208

Received June 20, 2002

The reaction of $Ru_5(CO)_{15}(\mu_5\text{-}C)$, **1**, with Ph_3SnH in the presence of UV irradiation has yielded the Ph_3SnH adduct $Ru_5(CO)_{15}(SnPh_3)(\mu_5\text{-}C)(\mu\text{-}H)$, **3**, by SnH bond activation and cleavage of one Ru–Ru bond in the cluster of **1**. The reaction of **1** with Ph_3SnH at 127 °C yielded the high nuclearity cluster compound $Ru_5(CO)_{10}(SnPh_3)(\mu\text{-}SnPh_2)_4(\mu_5\text{-}C)(\mu\text{-}H)$, **4**, that contains five tin ligands. Four of these are $SnPh_2$ groups that bridge each edge of the base of the Ru_5 square pyramidal cluster. The reaction of Ph_3SnH with the benzene-substituted cluster $Ru_5(CO)_{12}(C_6H_6)(\mu_5\text{-}C)$, **2**, at 68 °C yielded two products: $Ru_5(CO)_{11}(SnPh_3)(C_6H_6)(\mu_5\text{-}C)(\mu\text{-}H)$, **5**, and $Ru_5(CO)_{10}(SnPh_3)_2(C_6H_6)(\mu_5\text{-}C)(\mu\text{-}H)_2$, **6**. Both contain square pyramidal Ru_5 clusters with one and two $SnPh_3$ groups, respectively. At 127 °C, the reaction of **2** with an excess of Ph_3SnH has led to the formation of two new high-nuclearity cluster complexes: $Ru_5(CO)_8(\mu\text{-}SnPh_2)_4(C_6H_6)(\mu_5\text{-}C)$, **7**, and $Ru_5(CO)_7(\mu\text{-}SnPh_2)_4(SnPh_3)(C_6H_6)(\mu_5\text{-}C)(\mu\text{-}H)$, **8**. Both compounds contain square pyramidal Ru_5 clusters with $SnPh_2$ groups bridging each edge of the square base. Compound **8** contains a $SnPh_3$ group analogous to that of compound **4**. When treated with CO, compound **8** is converted to **4**. When heated to 68 °C, compound **5** was converted to the new compound $Ru_5(CO)_{11}(C_6H_6)(\mu_4\text{-}SnPh)(\mu_3\text{-}CPh)$, **9**, by loss of benzene and the shift of a phenyl group from the tin ligand to the carbido carbon atom to form a triply bridging benzylidyne ligand and a novel quadruply bridging stannylyne ligand.

Introduction

Recently, there has been much interest in synthesizing bimetallic nanoparticles from bimetallic molecular clusters.[1−8] Bimetallic nanoparticles have been shown to exhibit superior properties as catalysts.[8,9] Over the years, metal−tin compounds have attracted attention because tin is often used as one component in many bimetallic catalysts.[9,10] Tin complexes of palladium and platinum have been shown to be superior catalysts for hydrogenation and hydroformylation of olefins.[11] Ruthenium−tin carbonyl clusters have recently been shown to be precursors to bimetallic catalysts that exhibit superior selectivity in the hydrogenation of cyclic polyenes.[10] Ruthenium carbonyl cluster complexes containing tin ligands have been prepared by the addition of $SnCl_2$ and tertiary stannanes to suitable ruthenium carbonyl cluster complexes.[12,13]

Pentaruthenium carbido carbonyl cluster complexes have been the focus of considerable interest to cluster chemists.[14]

* To whom correspondence should be addressed. E-mail: Adams@mail.chem.sc.edu.

(1) Toshima, N.; Yonezawa, T. *New J. Chem.* **1998**, 1179.
(2) Johnson, B. F. G. *Coord. Chem. Rev.* **1999**, *192*, 1269.
(3) Midgley, P. A.; Weyland, M.; Thomas, J. M.; Johnson, B. F. G. *Chem. Commun.* **2001**, 907.
(4) Nashner, M. S.; Frenkel, A. I.; Somerville, D.; Hills, C. W.; Shapley, J. R.; Nuzzo, R. G. *J. Am. Chem. Soc.* **1998**, *120*, 8093.
(5) Nashner, M. S.; Frenkel, A. I.; Adler, D. L.; Shapley, J. R.; Nuzzo, R. G. *J. Am. Chem. Soc.* **1997**, *119*, 7760.
(6) Shephard, D. S.; Maschmeyer, T.; Johnson, B. F. G.; Thomas, J. M.; Sankar, G.; Ozkaya, D.; Zhou, W.; Oldroyd, R. D.; Bell, R. G. *Angew. Chem., Int. Ed. Engl.* **1997**, *36*, 2242.
(7) Raja, R.; Sankar, G.; Hermans, S.; Shephard, D. S.; Bromley, S.; Thomas, J. M.; Johnson, B. F. G. *Chem. Commun.* **1999**, 1571.
(8) (a) Raja, R.; Khimyak, T.; Thomas, J. M.; Hermans, S.; Johnson, B. F. G. *Angew. Chem., Int. Ed.* **2001**, *40*, 4639. (b) Shephard, D. S.; Maschmeyer, T.; Sankar, G.; Thomas, J. M.; Ozkaya, D.; Johnson, B. F. G.; Raja, R.; Oldroyd, R. D.; Bell, R. G. *Chem.—Eur. J.* **1998**, *4*, 1214.
(9) Sinfelt, J. H. *Bimetallic Catalysts. Discoveries, Concepts and Applications*; Wiley: New York, 1983.
(10) (a) Hermans, S.; Raja, R.; Thomas, J. M.; Johnson, B. F. G.; Sankar, G.; Gleeson, D. *Angew. Chem., Int. Ed.* **2001**, *40*, 1211. (b) Hermans, S.; Johnson, B. F. G. *Chem. Commun.* **2000**, 1955.
(11) Holt, M. S.; Wilson, W. L.; Nelson, J. H. *Chem. Rev.* **1989**, *89*, 11.
(12) (a) Brivio, E.; Ceriotti, A.; Garlaschelli, L.; Manassero, M.; Sansoni, M. *J. Chem. Soc., Chem. Commun.* **1995**, 2055. (b) Hermans, S.; Johnson, B. F. G. *Chem. Commun.* **2000**, 1955.

10.1021/ic0204169 CCC: $22.00
Published on Web 09/24/2002

These compounds engage in facile cluster-opening ligand addition reactions. We have now found that these clusters readily react with triphenylstannane through multiple additions to introduce large numbers of tin-containing ligands into $Ru_5(CO)_{15}(\mu_5\text{-C})$, **1**,[15] and $Ru_5(CO)_{12}(C_6H_6)(\mu_5\text{-C})$, **2**.[16] These reactions have yielded a number of new ruthenium−tin complexes with a wide range of ruthenium−tin compositions. These results are reported herein. A preliminary report of this work has been published.[17]

Experimental Section

General Data. All reactions were performed under a nitrogen atmosphere. Reagent grade solvents were dried by the standard procedures and were freshly distilled prior to use. Infrared spectra were recorded on a Nicolet 5DXBO FTIR spectrophotometer. ^{1}H NMR spectra were recorded on a Varian Inova 400 spectrometer operating at 400.16 MHz. Elemental analyses were performed by Desert Analytics (Tucson, AZ). Ph_3SnH was purchased from Alfa Products and was used without further purification. $Ru_5(CO)_{15}(\mu_5\text{-C})$[15] and $Ru_5(CO)_{12}(C_6H_6)(\mu_5\text{-C})$[16] were prepared according to the published procedures. Product separations were performed by TLC in air on Analtech 0.25 and 0.5 mm silica gel 60 Å F_{254} glass plates.

Synthesis of $Ru_5(CO)_{15}(SnPh_3)(\mu_5\text{-C})(\mu\text{-H})$, 3. A 25.0 mg amount of $Ru_5(CO)_{15}(\mu_5\text{-C})$ (0.027 mmol) was dissolved in 30 mL of hexane in a 50 mL three-neck round-bottom flask equipped with a reflux condenser and a stir bar. To this solution was added 47.0 mg (0.13 mmol) of Ph_3SnH. The reaction mixture was irradiated (medium pressure mercury lamp at 360 W) for 2 h. The solvent was then removed in vacuo, and the product was isolated by TLC using 4:1 hexane/methylene chloride solvent mixture to yield 7.5 mg (22%) of a yellow product, $Ru_5(CO)_{15}(SnPh_3)(\mu_5\text{-C})(\mu\text{-H})$ **(3).** Spectral data for **3**: IR ν_{CO} (cm^{-1} in hexane) 2105 (vw), 2072 (s), 2061 (s), 2026 (m), 2004 (m), 1993 (vw); ^{1}H NMR ($CDCl_3$ in ppm) δ = 7.3−7.7 (m, 15H, Ph), δ = −22.31 (s, 1H, hydride). Anal. Calcd: C, 31.69; H, 1.25. Found: C, 32.06; H, 1.33.

Synthesis of $Ru_5(CO)_{10}(SnPh_3)(\mu\text{-}SnPh_2)_4(\mu_5\text{-C})(\mu\text{-H})$, 4. A 11.2 mg amount of **1** (0.013 mmol) was dissolved in 15 mL of octane in a 50 mL three-neck round-bottom flask equipped with a stir bar. To this solution was added 27.8 mg of Ph_3SnH (0.073 mmol) dissolved in 10 mL octane, and this mixture was brought to reflux for 30 min. After cooling, the solvent was then removed in vacuo, and the product was purified by TLC using a 2:1 hexane/methylene chloride solvent mixture to yield 1.7 mg (6%) of a red product, $Ru_5(CO)_{10}(SnPh_3)(\mu\text{-}SnPh_2)_4(\mu_5\text{-C})(\mu\text{-H})$ **(4)**. Although the yield of **4** is low, no starting material **1** was recovered, and no other characterizable products could be isolated from this reaction. Spectral data for **4**: IR ν_{CO} (cm^{-1} in hexane) 2042 (w), 2022 (s), 2008 (vs), 1979 (m), 1963 (m), 1956 (m); ^{1}H NMR ($CDCl_3$ in ppm) δ = 6.70−8.05 (m, 55H, Ph), δ = −23.31 (s, 1H, hydride). Anal. Calcd: C, 41.27; H, 2.46. Found: C, 41.47; H, 2.35.

Reaction of 2 with Ph_3SnH at 68 °C. A 48.0 mg amount of **2** (0.052 mmol) was dissolved in 60 mL of hexane in a 100 mL three-neck round-bottom flask equipped with a stir bar. To this solution was added 90.0 mg of Ph_3SnH (0.26 mmol) dissolved in 15 mL of hexane, and this mixture was heated to reflux for 45 min. After cooling, the solvent was then removed in vacuo, and the products were purified by TLC using a 4:1 hexane/methylene chloride solvent mixture to yield 17.2 mg (26%) of a brown-red product, $Ru_5(CO)_{11}(SnPh_3)(C_6H_6)(\mu_5\text{-C})(\mu\text{-H})$ **(5)** and 6.6 mg (8%) of a red product, $Ru_5(CO)_{10}(SnPh_3)_2(C_6H_6)(\mu_5\text{-C})(\mu\text{-H})_2$ **(6)**. Spectral data for **5**: IR ν_{CO} (cm^{-1} in hexane) 2081 (s), 2052 (vs), 2036 (vs), 2020 (s), 2007 (m), 1999 (s), 1987 (w), 1942 (vw); ^{1}H NMR ($CDCl_3$ in ppm) δ = 7.29−7.54 (m, 15H, Ph), 5.46 (s, 6H, C_6H_6), −21.75 (s, 1H, hydride). Anal. Calcd: C, 34.44; H, 1.75. Found: C, 34.15; H, 1.58. Spectral data for **6**: IR ν_{CO} (cm^{-1} in hexane) 2087 (vs), 2081 (w), 2061 (vs), 2031 (m), 2024 (vs), 2009 (m), 2000 (m), 1984 (w), 1963 (w), 1943 (w); ^{1}H NMR ($CDCl_3$ in ppm) δ = 7.28−7.69 (m, 30H, Ph), 5.59 (s, 6H, C_6H_6), −19.68 (d, 1H, $^1J_{H-H}$ = 2.8, hydride), −20.70 (d, 1H, $^1J_{H-H}$ = 2.8, hydride). Anal. Calcd: C, 40.32; H, 2.41. Found: C, 40.62; H, 2.41.

Reaction of 2 with Ph_3SnH at 127 °C. A 9.3 mg amount of **2** (0.010 mmol) was dissolved in 10 mL of octane in a 50 mL three-neck round-bottom flask equipped with a stir bar. To this solution was added 15.2 mg of Ph_3SnH (0.043 mmol) dissolved in 5 mL of octane, and this mixture was brought to reflux for 20 min. After cooling, the solvent was then removed in vacuo, and the products were separated by TLC using a 2:1 hexane/methylene chloride solvent mixture to yield 0.5 mg (2%) of a red product, $Ru_5(CO)_8(C_6H_6)(\mu\text{-}SnPh_2)_4(\mu_5\text{-C})$ **(7)** and 6.2 mg (26%) of a red product, $Ru_5(CO)_7(SnPh_3)(C_6H_6)(\mu\text{-}SnPh_2)_4(\mu_5\text{-C})(\mu\text{-H})$ **(8)**. No other characterizable products were obtained. Spectral data for **7**: IR ν_{CO} (cm^{-1} in CH_2Cl_2) 2056 (w), 2024 (w), 2000 (m), 1977 (s), 1937 (s); ^{1}H NMR ($CDCl_3$ in ppm) δ = 7.28−7.95 (m, 40H, Ph), 4.35 (s, 6H, C_6H_6). MS: parent ion m/z = 1912. Spectral data for **8**: IR ν_{CO} (cm^{-1} in CH_2Cl_2) 2008 (s), 1987 (s), 1943 (s), 1928 (m, sh); ^{1}H NMR ($CDCl_3$ in ppm): δ = 6.70−8.05 (m, 55H, Ph), 4.48 (s, 6H, C_6H_6), −25.63 (s, 1H, hydride). Anal. Calcd: C, 42.99; H, 2.78. Found: C, 43.11; H, 2.64.

Thermolysis of 3. A 10.0 mg amount of **5** (0.008 mmol) was dissolved in 25 mL of hexane in a 50 mL three-neck round-bottom flask and was brought to reflux for 45 min. After cooling, the solvent was then removed in vacuo, and the product was purified by TLC using a 3:1 hexane/methylene chloride solvent mixture to yield 6.4 mg (68%) of a dark red product, $Ru_5(CO)_{11}(C_6H_6)(\mu_4\text{-SnPh})(\mu_3\text{-CPh})$ **(9)**. The product starts to decompose on the TLC plate, so the separation was done quickly. Spectral data: IR ν_{CO} (cm^{-1} in hexane) 2063 (s), 2033 (vs), 2020 (vs), 1999 (m), 1989 (sh), 1982 (m), 1961 (w), 1925 (w); ^{1}H NMR ($CDCl_3$ in ppm) δ = 7.36−7.68 (m, 10H, Ph), 5.48 (s, 6H, C_6H_6). Anal. Calcd: C, 30.60; H, 1.36. Found: C, 30.98; H, 1.27.

Conversion of 8 to 4 by Reaction with CO. A 10.0 mg amount of **8** (0.005 mmol) was dissolved in 8 mL of toluene in a stainless steel Parr pressure reactor. The reactor was pressurized with 45 atm of CO, placed in an oil bath maintained at 100 °C, and allowed to stir for 2 h. The solvent was then removed in vacuo and the product purified by TLC using a 2:1 hexane/methylene chloride solvent mixture to yield 5.3 mg (53%) of **4**.

Crystallographic Analysis. Orange single crystals of **3** and red single crystals of **4** suitable for diffraction analysis were grown by slow evaporation of solvent from a solution in a hexane/methylene chloride solvent mixture at −20 °C and from a cyclohexane solution

(13) (a) Cabeza, J. A.; Del Rio, I.; Riera, V. *Inorg. Chim. Acta* **1998**, *268*, 131. (b) Bois, C.; Cabeza, J. A.; Franco, R. J.; Riera, V.; Saborit, E. *J. Organomet. Chem.* **1998**, *564*, 201. (c) Cabeza, J. A.; Llamazares, A.; Riera, V.; Triki, S.; Ouahab, L. *Organometallics* **1992**, *11*, 3334. (d) Cabeza, J. A.; Garcia-Granda, S.; Llamazares, A.; Riera, V.; Van der Maelen, J. F. *Organometallics* **1993**, *12*, 157. (e) Cabeza, J. A.; Franco, R. J.; Riera, V.; Garcia-Granda, S.; Van der Maelen, J. F. *Organometallics* **1995**, *14*, 3342.
(14) Dyson, P. J. *Adv. Organomet. Chem.* **1999**, *43*, 43.
(15) Nicholls, J. N.; Vargas, M. D.; Hriljac, J.; Sailor, M. *Inorg. Synth.* **1989**, *26*, 283.
(16) Braga, D.; Grepioni, F.; Sabatino, P.; Dyson, P. J.; Johnson, B. F. G.; Lewis, J.; Bailey, P. J.; Raithby, P. R.; Stalke, D. *J. Chem. Soc., Dalton Trans.* **1993**, 985.
(17) Adams, R. D.; Captain, B.; Fu. W.; Smith, M. D. *Inorg. Chem.* **2002**, *41*, 2302.

at 5 °C, respectively. Dark red single crystals of **5** and red single crystals of **6** suitable for diffraction analysis were grown by slow evaporation of solvent from a hexane/methylene chloride solution and a benzene/octane solution, respectively, at 5 °C. Red single crystals of **7** and **8** were grown by slow evaporation of solvent from solutions in a hexane/methylene chloride solvent mixture at −20 °C and 5 °C, respectively. Dark red single crystals of **9** were grown by slow evaporation of solvent from a diethyl ether solution at −20 °C. For compound **3**, the crystal used for the diffraction measurements was mounted in a thin-walled glass capillary. Diffraction measurements were made on a Rigaku AFC6S fully automated four-circle diffractometer. The unit cell was determined and refined from 15 randomly selected reflections. The calculations were performed on a Silicon Graphic Indigo 2 computer by using the TEXSAN motif structure solving program library. Neutral atom scattering factors were calculated by the standard procedures.[18a] Anomalous dispersion corrections were applied to all non-hydrogen atoms.[18b] Lorentz/polarization (Lp) and absorption corrections were applied to the data for each structure. Full-matrix least-squares refinements minimized the function $\sum_{hkl} w(|F_o| - |F_c|)^2$, where $w = 1/\sigma^2(F)$, $\sigma(F) = \sigma(F_o^2)/2F_o$, and $\sigma(F_o^2) = [(\sigma I_{raw})^2 + (0.06)I_{net})^2]^{1/2}$/Lp. The structure was solved by a combination of direct methods (SIR 92) and difference Fourier syntheses.

For compounds **4**−**9**, the data crystals were glued onto the end of a thin glass fiber. X-ray intensity data were measured using a Bruker SMART APEX CCD-based diffractometer using Mo Kα radiation ($\lambda = 0.71073$ Å). The unit cells were initially determined on the basis of reflections selected from a set of three scans measured in orthogonal wedges of reciprocal space. The raw data frames were integrated with the SAINT+ program using a narrow-frame integration algorithm.[19] Correction for the Lorentz and polarization effects were also applied by SAINT. An empirical absorption correction based on the multiple measurement of equivalent reflections was applied by using the program SADABS. These structures were solved by a combination of direct methods and difference Fourier syntheses and refined by full-matrix least-squares on F^2, using the SHELXTL software package.[20] Crystal data, data collection parameters, and results of the analyses for compounds **3** and **4** are listed in Table 1, for compounds **5** and **6** are listed in Table 2, and for compounds **7**−**9** are listed in Table 3.

Results and Discussion

The reaction of $Ru_5(CO)_{15}(\mu_5\text{-C})$, **1**, with Ph_3SnH at room temperature in the presence of UV irradiation has yielded the new compound $Ru_5(CO)_{15}(SnPh_3)(\mu_5\text{-C})(\mu\text{-H})$, **3**, in 22% yield. Compound **3** was characterized by a combination of IR, NMR, and single-crystal X-ray diffraction analysis. Compound **3** crystallizes with two independent formula equivalents of the molecule in the asymmetric crystal unit. Both molecules are structurally similar, and an ORTEP diagram of the molecular structure of one of these is shown in Figure 1. Selected bond distances and angles are listed in Table 4. This compound contains an open $Ru_5(\mu_5\text{-C})$ cluster where one ruthenium atom bridges the wingtips of an Ru_4C butterfly cluster arrangement. The triphenyltin group is coordinated to that bridging ruthenium atom, Ru(1), and the Ru(1)−Sn(1) of 2.7226(9) Å is typical of a Ru−Sn single bond. The hydride ligand, located and refined structurally, bridges the hinge bond, Ru(3)−Ru(4), of the Ru_4 butterfly, and it exhibits the usual high-field resonance, $\delta = -22.31$ ppm in the ^{1}H NMR spectrum of the compound. The

Table 1. Crystallographic Data for Compounds **3** and **4**

	3	**4**
empirical formula	$Ru_5Sn_2O_{15}C_{34}H_{16}$	$Ru_5Sn_5O_{10}C_{77}H_{55}$
fw	2577.06	2239.01
cryst syst	triclinic	monoclinic
lattice params		
a (Å)	18.040(1)	24.709(2)
b (Å)	9.157(1)	22.389(2)
c (Å)	24.528(3)	19.3966(18)
α (deg)	90.23(1)	90
β (deg)	93.08(1)	99.076(2)
γ (deg)	89.81(1)	90
V (Å^3)	4046.0(6)	10595.9(17)
space group	$P\bar{1}$	$C2/m$
Z value	4	4
ρ_{calcd} (g/cm^3)	2.12	1.404
μ (Mo Kα) (mm^{-1})	2.492	1.887
T (K)	293	296
no. observations	7798 ($I > 3\sigma(I)$)	5756 ($I > 2\sigma(I)$)
no. params	1000 (no. variables)	447
GOF	1.35	0.962
max shift in cycle	0.02	0.001
residuals R1; wR2[a]	0.030; 0.052	0.0582; 0.1657
abs correction, max/min	DIFABS, 1.00/0.57	SADABS, 1.000/0.679
largest peak in final diff map (e$^-$/Å^3)	0.59	2.271

[a] $R = \sum_{hkl}(||F_o| - |F_c||)/\sum_{hkl}|F_o|$; $R_w = [\sum_{hkl} w(|F_o| - |F_c|)^2/\sum_{hkl} wF_o^2]^{1/2}$, $w = 1/\sigma^2(F_o)$; GOF $= [\sum_{hkl}(w(|F_o| - |F_c|))^2/(n_{data} - n_{vari})]^{1/2}$. R1 $= \sum(||F_o| - |F_c||)/\sum|F_o|$. wR2 $= \{\sum[w(F_o^2 - F_c^2)^2/\sum[w(F_o^2)^2]\}^{1/2}$; $w = 1/\sigma^2(F_o^2)$. GOF $= [\sum_{hkl}(w(|F_o^2| - |F_c^2|))^2/(n_{data} - n_{vari})]^{1/2}$.

Table 2. Crystallographic Data for Compounds **5** and **6**

	5	**6**
empirical formula	$Ru_5SnO_{11}C_{36}H_{22}$	$Ru_5Sn_2O_{10}C_{53}H_{38}\cdot 2C_6H_6\cdot 2^1/_2C_8H_{18}$
fw	1254.58	1790.89
cryst syst	monoclinic	triclinic
lattice params		
a (Å)	12.3859(7)	13.8064(8)
b (Å)	18.8897(11)	15.4231(9)
c (Å)	17.2928(10)	16.4974(10)
α (deg)	90	100.5060(10)
β (deg)	106.643(1)	95.8230(10)
γ (deg)	90	105.2120(10)
V (Å^3)	3876.4(4)	3291.5(3)
space group	$P2_1/n$	$P\bar{1}$
Z value	4	2
ρ_{calcd} (g/cm^3)	2.150	1.807
μ (Mo Kα) (mm^{-1})	2.590	1.919
T (K)	293	190
no. params	483	760
GOF	1.002	1.001
max shift in cycle	0.002	0.001
residuals R1; wR2[a]	0.0225; 0.0478	0.0366; 0.0824
abs correction, max/min	SADABS, 0.745/0.346	SADABS, 0.928/0.820
largest peak in final diff map (e$^-$/Å^3)	0.618	1.333

[a] $R = \sum_{hkl}(||F_o| - |F_c||)/\sum_{hkl}|F_o|$; $R_w = [\sum_{hkl} w(|F_o| - |F_c|)^2/\sum_{hkl} wF_o^2]^{1/2}$, $w = 1/\sigma^2(F_o)$; GOF $= [\sum_{hkl}(w(|F_o| - |F_c|))^2/(n_{data} - n_{vari})]^{1/2}$. R1 $= \sum(||F_o| - |F_c||)/\sum|F_o|$. wR2 $= \{\sum[w(F_o^2 - F_c^2)^2/\sum[w(F_o^2)^2]\}^{1/2}$; $w = 1/\sigma^2(F_o^2)$. GOF $= [\sum_{hkl}(w(|F_o^2| - |F_c^2|))^2/(n_{data} - n_{vari})]^{1/2}$.

(18) (a) *International Tables for X-ray Crystallography*; Kynoch Press: Birmingham, U.K., 1975; Vol. IV, Table 2.2B, pp 99−101. (b) *International Tables for X-ray Crystallography*; Kynoch Press: Birmingham, U.K., 1975; Vol. IV, Table 2.3.1, pp 149−150.
(19) *SAINT+*, Version 6.02a; Bruker Analytical X-ray System, Inc.: Madison, WI, 1998.
(20) Sheldrick, G. M. *SHELXTL*, Version 5.1; Bruker Analytical X-ray Systems, Inc.: Madison, WI, 1997.

Table 3. Crystallographic Data for Compounds **7**−**9**

	7	**8**	**9**
empirical formula	$Ru_5Sn_4O_8C_{63}H_{46}$·$1.0C_6H_{14}$·$^1/_4CH_2Cl_2$	$Ru_5Sn_5O_7C_{80}$-H_{61}·$^1/_4C_6H_{14}$	$Ru_{10}Sn_2O_{22}C_{60}$ H_{32}·$1.0OC_4H_{10}$
fw	2018.51	2276.17	2427.06
cryst syst	monoclinic	orthorhombic	triclinic
lattice params			
a (Å)	14.6107 (11)	20.3739 (10)	9.7219 (7)
b (Å)	18.7109 (14)	22.1686 (11)	17.0961 (12)
c (Å)	25.3931 (19)	19.0630 (9)	23.3176 (16)
α (deg)	90	90	70.876 (2)
β (deg)	102.8120(10)	90	83.645 (2)
γ (deg)	90	90	76.101 (2)
V (Å^3)	6769.1 (9)	8610.0 (7)	3552.3 (4)
space group	$P2_1/c$	*Pnma*	$P\bar{1}$
Z value	4	4	2
ρ_{calcd} (g/cm^3)	1.981	1.756	2.269
μ (Mo Kα) (mm^{-1})	2.604	2.322	2.822
T (K)	190	293	293
no. observations ($I > 2\sigma(I)$)	9944	5966	6033
no. params	789	498	894
GOF	1.143	1.093	1.003
max shift in cycle	0.108	0.001	0.001
residuals R1; wR2[a]	0.0595; 0.1488	0.0469; 0.1196	0.0496; 0.0894
abs correction, max/min	SADABS 0.694/0.571	SADABS 0.962/0.804	SADABS 0.693/0.559
largest peak in final diff map (e$^-$/Å^3)	1.535	0.952	1.080

[a] $R = \sum_{hkl}(||F_o| - |F_c||)/\sum_{hkl}|F_o|$; $R_w = [\sum_{hkl}w(|F_o| - |F_c|)^2/\sum_{hkl}wF_o^2]^{1/2}$, $w = 1/\sigma^2(F_o)$; GOF $= [\sum_{hkl}(w(|F_o| - |F_c|))^2/(n_{data} - n_{vari})]^{1/2}$. R1 $= \sum(||F_o| - |F_c||)/\sum|F_o|$. wR2 $= \{\sum[w(F_o^2 - F_c^2)^2/\sum[w(F_o^2)^2]\}^{1/2}$; $w = 1/\sigma^2(F_o^2)$. GOF $= [\sum_{hkl}(w(|F_o^2| - |F_c^2|))^2/(n_{data} - n_{vari})]^{1/2}$.

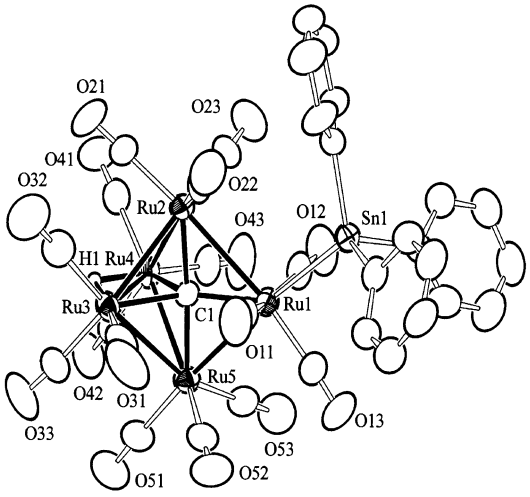

Figure 1. ORTEP diagram of the molecular structure of $Ru_5(CO)_{15}$-$(SnPh_3)(\mu_5\text{-C})(\mu\text{-H})$, **3**, showing 40% thermal ellipsoid probability.

structure of the cluster of **3** is similar to that of the previously reported open Ru_5 cluster compound, $Ru_5(CO)_{15}(NCMe)$-$(\mu_5\text{-C})$,[21] and its silyl homologue $Ru_5(CO)_{15}(SiEt_3)(\mu_5\text{-C})(\mu$-H).[22] Compound **3** was formed by an oxidative addition of the tin−hydrogen bond to **1** with a cleavage of one of the apical−equatorial Ru−Ru bonds of the square pyramidal cluster, eq 1.[22] Unlike the silyl compound $Ru_5(CO)_{15}(SiEt_3)$-

(21) (a) Johnson, B. F. G.; Lewis, J.; Nicholls, J. N.; Puga, J.; Raithby, P. R.; Rosales, M. J.; McPartlin, M.; Clegg, W. *J. Chem. Soc., Dalton Trans.* **1983**, 277. (b) Farrar, D. H.; Poë, A. J.; Zheng, Y. *J. Am. Chem. Soc.* **1994**, *116*, 6252.

(22) Adams, R. D.; Captain, B.; Fu, W. *Organometallics* **2000**, *19*, 3670.

Table 4. Selected Intramolecular Distances and Angles for $Ru_5(CO)_{15}(SnPh_3)(\mu_5\text{-C})(\mu\text{-H})$, **3**[a]

Distances

atom	atom	distance (Å)	atom	atom	distance (Å)
Ru(1)	Ru(2)	2.9756(9)	Ru(1)	C(1)	2.146(8)
Ru(1)	Ru(5)	2.953(1)	Ru(2)	C(1)	1.953(8)
Ru(2)	Ru(3)	2.870(1)	Ru(3)	C(1)	2.125(8)
Ru(2)	Ru(4)	2.843(1)	Ru(4)	C(1)	2.128(8)
Ru(3)	Ru(4)	2.830(1)	Ru(5)	C(1)	1.976(8)
Ru(3)	Ru(5)	2.844(1)	Ru(3)	H(1)	1.81(8)
Ru(4)	Ru(5)	2.857(1)	Ru(4)	H(1)	1.60(8)
Ru(1)	Sn(1)	2.7226(9)	C	O(av)	1.13(1)

Angles

atom	atom	atom	angle (deg)	atom	atom	atom	angle (deg)
Ru(2)	Ru(1)	Ru(5)	82.94(3)	Ru(2)	Ru(4)	Ru(5)	87.07(3)
Ru(1)	Ru(2)	Ru(3)	86.14(3)	Ru(1)	Ru(5)	Ru(3)	87.12(2)
Ru(1)	Ru(2)	Ru(4)	86.61(3)	Ru(1)	Ru(5)	Ru(4)	86.79(3)
Ru(2)	Ru(3)	Ru(5)	86.81(3)	Ru(2)	Ru(1)	Sn(1)	102.24(3)
Ru(5)	Ru(1)	Sn(1)	174.69(6)	Ru	C	O(av)	175(1)

[a] Estimated standard deviations in the least significant figure are given in parentheses.

$(\mu_5\text{-C})(\mu\text{-H})$ which eliminates CO when heated to close the cluster,[22] compound **3** decomposed when heated, and no characterizable compounds could be isolated.

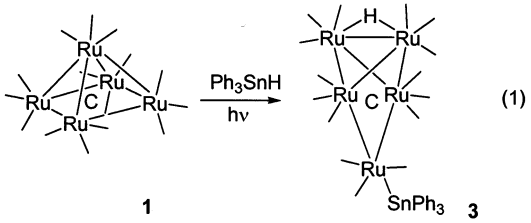

Interestingly, the thermal reaction of **1** with an excess of Ph_3SnH at 127 °C does not yield **3** but leads instead to the formation of the new high nuclearity compound $Ru_5(CO)_{10}$-$(SnPh_3)(\mu\text{-}SnPh_2)_4(\mu_5\text{-C})(\mu\text{-H})$, **4**, in a 6% yield. Although the yield of **4** is low, no starting material **1** was recovered, and no other characterizable products could be isolated from this reaction. Compound **4** was characterized by a combina-

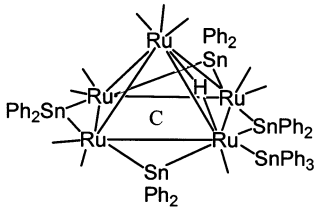

4

tion of IR, NMR, and single-crystal X-ray diffraction analysis. An ORTEP diagram of the molecular structure of **4** is shown in Figure 2. Selected bond distances and angles are listed in Table 5. Compound **4** contains a square pyramidal cluster of five ruthenium atoms with a carbon atom located in the center of the base of the square pyramid. Surprisingly, compound **4** contains five tin ligands. Four of these are in the form of $SnPh_2$ groups that bridge each of the four Ru−Ru edges of the square base of the cluster. The fifth tin-containing ligand is a $SnPh_3$ group that is terminally

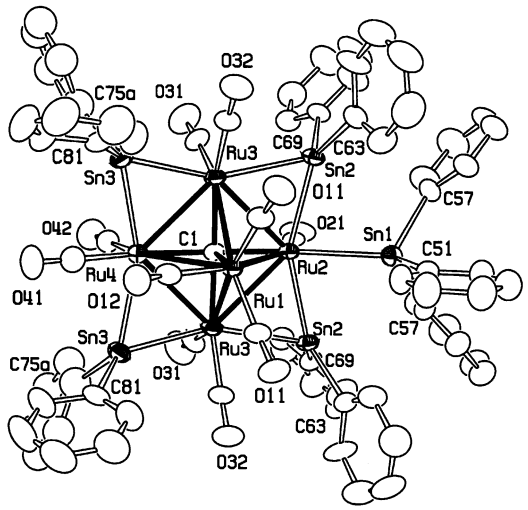

Figure 2. ORTEP diagram of the molecular structure of $Ru_5(CO)_{10}(\mu\text{-}SnPh_2)_4(SnPh_3)(\mu_5\text{-}C)(\mu_5\text{-}H)$, **4**, showing 40% thermal ellipsoid probability.

Table 5. Selected Intramolecular Distances and Angles for $Ru_5(CO)_{10}(\mu\text{-}SnPh_2)_4(SnPh_3)(\mu_5\text{-}C)(\mu\text{-}H)$, **4**[a]

Distances

atom	atom	distance (Å)	atom	atom	distance (Å)
Ru(1)	Ru(2)	2.9075(11)	Ru(3)	Sn(3)	2.6011(8)
Ru(1)	Ru(3)	2.8338(8)	Ru(4)	Sn(3)	2.6618(6)
Ru(1)	Ru(4)	2.9062(12)	Ru(1)	C(1)	2.153(9)
Ru(2)	Ru(3)	2.9135(8)	Ru(2)	C(1)	2.022(10)
Ru(3)	Ru(4)	2.8655(8)	Ru(3)	C(1)	2.0410(11)
Ru(2)	Sn(1)	2.7470(11)	Ru(4)	C(1)	2.087(10)
Ru(2)	Sn(2)	2.6134(5)	C	O(av)	1.13(1)
Ru(3)	Sn(2)	2.7303(8)			

Angles

atom	atom	atom	angle (deg)	atom	atom	atom	angle (deg)
Ru(1)	Ru(2)	Ru(3)	58.26(2)	Ru(3)	Ru(2)	Sn(1)	131.92(2)
Ru(2)	Ru(3)	Ru(4)	90.50(2)	Ru(2)	Sn(2)	Ru(3)	66.04(2)
Ru(2)	Ru(1)	Ru(4)	89.82(3)	Ru(3)	Sn(3)	Ru(4)	65.97(3)
Ru(1)	Ru(2)	Sn(1)	116.02(4)	Ru	C	O(av)	176(1)

[a] Estimated standard deviations in the least significant figure are given in parentheses.

bonded to one of the basal atoms, Ru(2). The one bridging hydride ligand was not located crystallographically, but it is clearly indicated by its high-field resonance in the ^{1}H NMR spectrum, at $\delta = -23.31$ ppm. It is believed to bridge the long Ru−Ru bond, Ru(1)−Ru(2) = 2.9075(11) Å, proximate to the terminally coordinated $SnPh_3$ group. The Ru−Sn bond distance to the $SnPh_3$ ligand, Ru(2)−Sn(1) = 2.7470(11) Å, is similar to that found in **3** but is longer than those to the bridging $SnPh_2$ ligands which lie in the range 2.6011(8)−2.7303(8) Å.

The reaction of Ph_3SnH with the benzene-substituted pentaruthenium carbido cluster $Ru_5(CO)_{12}(C_6H_6)(\mu_5\text{-}C)$, **2**, at 68 °C yielded two products $Ru_5(CO)_{11}(SnPh_3)(C_6H_6)(\mu_5\text{-}C)(\mu\text{-}H)$, **5**, (26% yield) and $Ru_5(CO)_{10}(SnPh_3)_2(C_6H_6)(\mu_5\text{-}C)(\mu\text{-}H)_2$, **6**, (8% yield). Compounds **5** and **6** were both characterized by a combination of IR, NMR, and single-crystal X-ray diffraction analyses.

An ORTEP diagram of the molecular structure of **5** is shown in Figure 3. Selected bond distances and angles are listed in Table 6. Compound **5** was formed by the oxidative

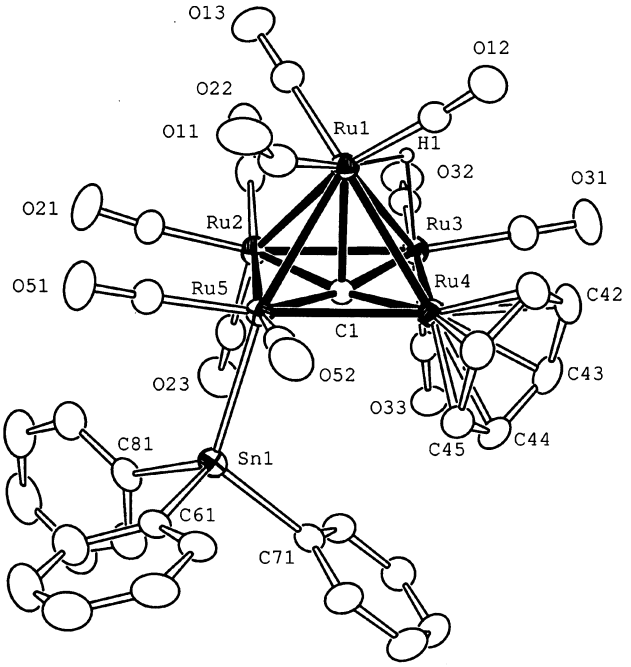

Figure 3. ORTEP diagram of the molecular structure of $Ru_5(CO)_{11}(SnPh_3)(C_6H_6)(\mu_5\text{-}C)(\mu\text{-}H)$, **5,** showing 40% thermal ellipsoid probability.

addition of 1 equiv of Ph_3SnH to **2**, and a loss of one CO ligand (eq 2).

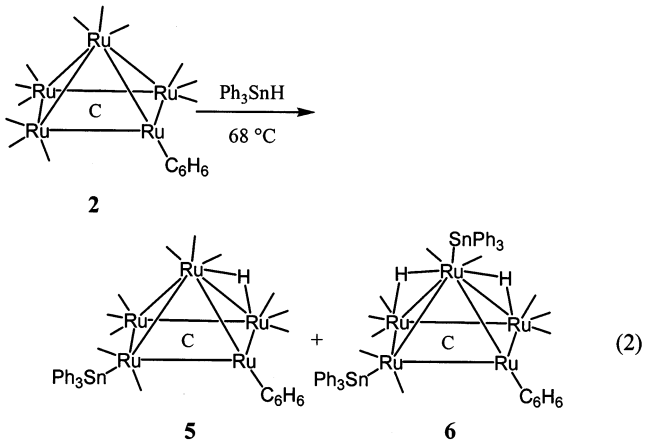

(2)

The structure of **5** consists of a square pyramidal Ru_5C cluster with one $SnPh_3$ ligand bonded terminally to the basal ruthenium atom, Ru(5), of the square pyramid. The Ru(5)−Sn(1) distance is significantly shorter, 2.6362(3) Å, than those found in **3** and **4**, but it is similar to that found in **6**, see later. The benzene ligand is coordinated to another basal ruthenium atom, Ru(4). The compound contains one hydride ligand that bridges across an apical−basal ruthenium bond, Ru(1)−Ru(3) = 2.8702(4) Å, $\delta = -21.75$ ppm.

Compound **6** was formed by the oxidative addition of 2 equiv of Ph_3SnH to **2**, and loss of two CO ligands (eq 2). An ORTEP diagram of the molecular structure of **6** is shown in Figure 4. Selected bond distances and angles are listed in Table 7. Like **5**, compound **6** also contains of a square pyramidal Ru_5C cluster, but it has two $SnPh_3$ ligands, one bonded terminally to the basal ruthenium atom, Ru(5), and one bonded terminally to the apical ruthenium atom,

Table 6. Selected Intramolecular Distances and Angles for $Ru_5(CO)_{11}(SnPh_3)(C_6H_6)(\mu_5\text{-}C)(\mu\text{-}H)$, **5**[a]

Distances

atom	atom	distance (Å)	atom	atom	distance (Å)
Ru(1)	Ru(2)	2.7990(4)	Ru(1)	C(1)	2.195(3)
Ru(1)	Ru(3)	2.8702(4)	Ru(2)	C(1)	2.030(3)
Ru(1)	Ru(4)	2.8538(4)	Ru(3)	C(1)	2.103(3)
Ru(1)	Ru(5)	2.9054(3)	Ru(4)	C(1)	1.893(3)
Ru(2)	Ru(3)	2.8264(4)	Ru(5)	C(1)	2.045(3)
Ru(2)	Ru(5)	2.8608(4)	Ru(1)	H(1)	1.77(3)
Ru(3)	Ru(4)	2.8327(4)	Ru(3)	H(1)	1.82(3)
Ru(4)	Ru(5)	2.8573(4)	C	O(av)	1.13(1)
Ru(5)	Sn(1)	2.6362(3)			

Angles

atom	atom	atom	angle (deg)	atom	atom	atom	angle (deg)
Ru(2)	Ru(1)	Ru(4)	87.527(10)	Ru(2)	Ru(5)	Ru(4)	86.287(9)
Ru(3)	Ru(1)	Ru(5)	91.333(10)	Ru(1)	Ru(5)	Sn(1)	153.470(11)
Ru(3)	Ru(2)	Ru(5)	93.171(9)	Ru(2)	Ru(5)	Sn(1)	101.718(10)
Ru(2)	Ru(3)	Ru(4)	87.412(9)	Ru(4)	Ru(5)	Sn(1)	105.891(10)
Ru(3)	Ru(4)	Ru(5)	93.114(9)	Ru	C	O(av)	175(3)

[a] Estimated standard deviations in the least significant figure are given in parentheses.

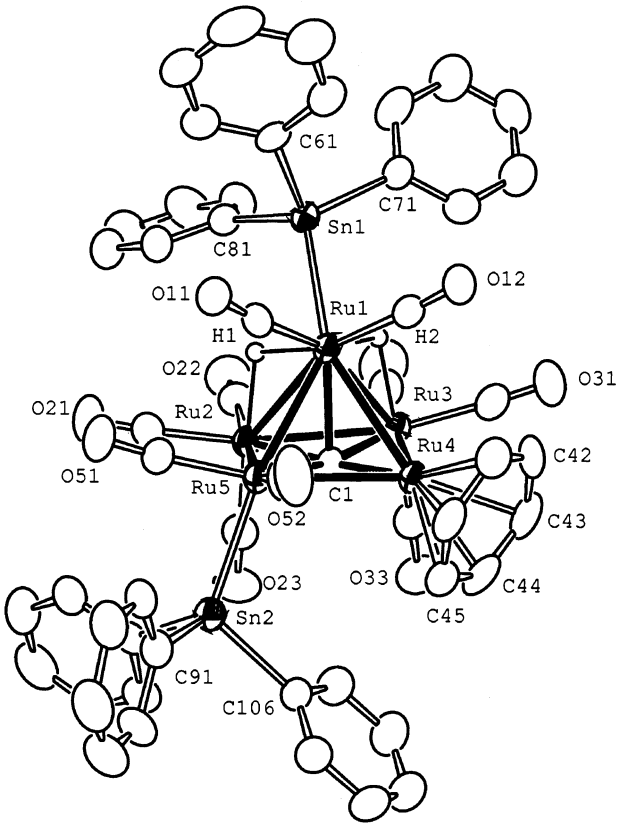

Figure 4. ORTEP diagram of the molecular structure of $Ru_5(CO)_{10}(SnPh_3)_2(C_6H_6)(\mu_5\text{-}C)(\mu\text{-}H)_2$, **6**, showing 40% thermal ellipsoid probability.

Ru(1). The Ru−Sn distances, Ru(1)−Sn(1) = 2.6652(5) Å, Ru(5)−Sn(2) = 2.6397(5) Å are both shorter than those in **3** and **4**. Note that the shorter of the two, Ru(5)−Sn(2), is bonded to a basal ruthenium atom. It is apparent from the diagram that this coordination site is sterically less crowded than the site of Sn(1). Reduced steric effects could thus explain why the Ru(5)−Sn(2) bond is shorter than the Ru(1)−Sn(1) bond. Similarly, reduced steric crowding could also explain why the Ru(5)−Sn(1) bond in **5** is short and

Table 7. Selected Intramolecular Distances and Angles for $Ru_5(CO)_{10}(SnPh_3)_2(C_6H_6)(\mu_5\text{-}C)(\mu\text{-}H)_2$, **6**[a]

Distances

atom	atom	distance (Å)	atom	atom	distance (Å)
Ru(1)	Ru(2)	2.8842(5)	Ru(1)	C(1)	2.167(5)
Ru(1)	Ru(3)	2.8314(6)	Ru(2)	C(1)	2.060(4)
Ru(1)	Ru(4)	2.9133(5)	Ru(3)	C(1)	2.107(5)
Ru(1)	Ru(5)	2.8976(6)	Ru(4)	C(1)	1.885(4)
Ru(2)	Ru(3)	2.8526(6)	Ru(5)	C(1)	2.031(4)
Ru(2)	Ru(5)	2.8939(6)	Ru(1)	H(1)	1.86(7)
Ru(3)	Ru(4)	2.8208(6)	Ru(2)	H(1)	1.74(7)
Ru(4)	Ru(5)	2.8513(5)	Ru(1)	H(2)	1.73(5)
Ru(1)	Sn(1)	2.6652(5)	Ru(3)	H(2)	1.85(6)
Ru(5)	Sn(2)	2.6397(5)	C	O(av)	1.13(1)

Angles

atom	atom	atom	angle (deg)	atom	atom	atom	angle (deg)
Ru(2)	Ru(1)	Ru(4)	85.671(15)	Ru(3)	Ru(1)	Sn(1)	108.780(17)
Ru(3)	Ru(1)	Ru(5)	91.988(16)	Ru(4)	Ru(1)	Sn(1)	155.906(18)
Ru(3)	Ru(2)	Ru(5)	91.631(16)	Ru(1)	Ru(5)	Sn(2)	159.656(19)
Ru(2)	Ru(3)	Ru(4)	88.016(16)	Ru(2)	Ru(5)	Sn(2)	103.828(17)
Ru(3)	Ru(4)	Ru(5)	93.190(16)	Ru(4)	Ru(5)	Sn(2)	109.241(17)
Ru(2)	Ru(5)	Ru(4)	86.639(16)	Ru	C	O(av)	175(3)
Ru(2)	Ru(1)	Sn(1)	106.358(16)				

[a] Estimated standard deviations in the least significant figure are given in parentheses.

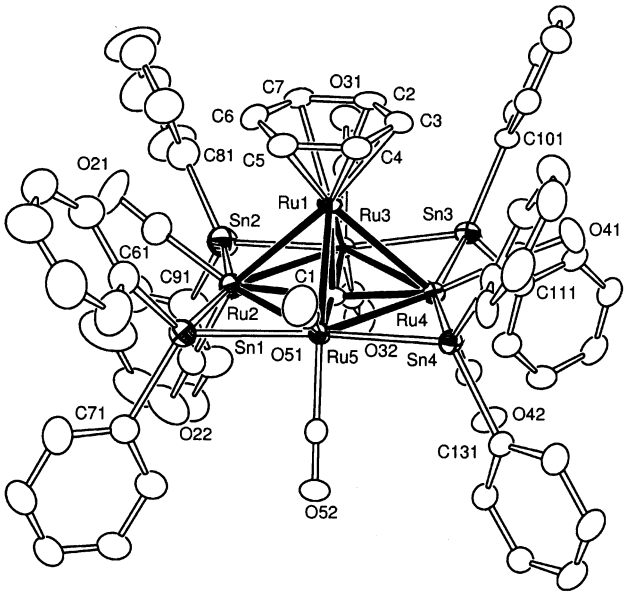

Figure 5. ORTEP diagram of the molecular structure of $Ru_5(CO)_8(C_6H_6)(\mu\text{-}SnPh_2)_4(\mu_5\text{-}C)$, **7**, showing 40% thermal ellipsoid probability.

very similar in length to those in **6**. The benzene ligand in **6** is coordinated to the basal ruthenium atom, Ru(4). There are two hydride ligands that bridge different apical−basal ruthenium bonds, Ru(1)−Ru(2) = 2.8842(5) Å, Ru(1)−Ru(3) = 2.8314(6) Å. These two hydride ligands (located and refined structurally) are inequivalent. This is confirmed by the observation of two mutually coupled high-field resonances in the ^{1}H NMR spectrum, $\delta = -19.68$ (d, 1H, $^1J_{H-H} = 2.8$ Hz), −20.70 (d, 1H, $^1J_{H-H} = 2.8$ Hz).

The reaction of **2** with an excess of Ph_3SnH at 127 °C has led to the formation of two new high-nuclearity cluster complexes: $Ru_5(CO)_8(C_6H_6)(\mu\text{-}SnPh_2)_4(\mu_5\text{-}C)$, **7**, in 2% yield and $Ru_5(CO)_7(SnPh_3)(C_6H_6)(\mu\text{-}SnPh_2)_4(\mu_5\text{-}C)(\mu\text{-}H)$, **8**, in 26% yield.[17] Compounds **7** and **8** were also both characterized

Scheme 1

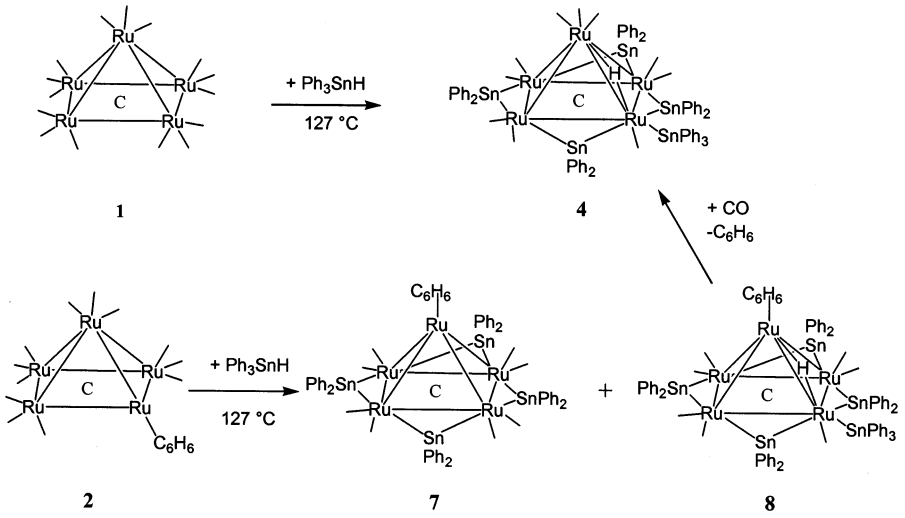

Table 8. Selected Intramolecular Distances and Angles for $Ru_5(CO)_8(\mu\text{-}SnPh_2)_4(C_6H_6)(\mu_5\text{-}C)$, **7**[a]

Distances

atom	atom	distance (Å)	atom	atom	distance (Å)
Ru(1)	Ru(2)	2.7633(11)	Ru(3)	Sn(3)	2.6239(11)
Ru(1)	Ru(3)	2.7701(10)	Ru(4)	Sn(3)	2.6280(10)
Ru(1)	Ru(4)	2.7922(11)	Ru(4)	Sn(4)	2.6261(9)
Ru(1)	Ru(5)	2.7673(10)	Ru(5)	Sn(1)	2.6429(11)
Ru(2)	Ru(3)	2.8825(12)	Ru(5)	Sn(4)	2.6278(10)
Ru(2)	Ru(5)	2.8864(11)	Ru(1)	C(1)	2.038(9)
Ru(3)	Ru(4)	2.9012(10)	Ru(2)	C(1)	2.053(10)
Ru(4)	Ru(5)	2.8983(11)	Ru(3)	C(1)	2.047(8)
Ru(2)	Sn(1)	2.6027(11)	Ru(4)	C(1)	2.051(10)
Ru(2)	Sn(2)	2.6022(12)	Ru(5)	C(1)	2.056(8)
Ru(3)	Sn(2)	2.6654(12)	C	O(av)	1.14(1)

Angles

atom	atom	atom	angle (deg)	atom	atom	atom	angle (deg)
Ru(2)	Ru(1)	Ru(4)	94.87(3)	Ru(2)	Sn(1)	Ru(5)	66.76(3)
Ru(3)	Ru(1)	Ru(5)	95.17(3)	Ru(2)	Sn(2)	Ru(3)	66.34(3)
Ru(3)	Ru(2)	Ru(5)	90.25(3)	Ru(3)	Sn(3)	Ru(4)	67.07(3)
Ru(2)	Ru(3)	Ru(4)	90.06(3)	Ru(4)	Sn(4)	Ru(5)	66.96(3)
Ru(3)	Ru(4)	Ru(5)	89.65(3)	Ru	C	O(av)	66.96(3)
Ru(2)	Ru(5)	Ru(4)	90.04(3)				177(1)

[a] Estimated standard deviations in the least significant figure are given in parentheses.

by a combination of IR, NMR and single-crystal X-ray diffraction analyses. An ORTEP diagram of the molecular structure of **7** is shown in Figure 5. Selected bond distances and angles are listed in Table 8. Compound **7** consists of a square pyramidal cluster of five ruthenium atoms with four bridging $SnPh_2$ groups, one on each edge of the base of the square pyramid, see Scheme 1. The benzene ligand has been relocated from a basal coordination site to the apical ruthenium atom, Ru(1). This relocation process is not unusual and has been also been observed to occur in the parent compound $Ru_5(CO)_{12}(C_6H_6)(\mu_5\text{-}C)$, **2**.[23] The Ru−Sn bond distances to the $SnPh_2$ bridging groups are similar to those in **4**, all lie in the range 2.6022(12)−2.6654(12) Å.

An ORTEP diagram of the molecular structure of **8** is shown in Figure 6. Selected bond distances and angles are

(23) Brown, B. B.; Dyson, P. J.; Johnson, B. F. G.; Parker, D. *J. Organomet. Chem.* **1995**, *491*, 189.

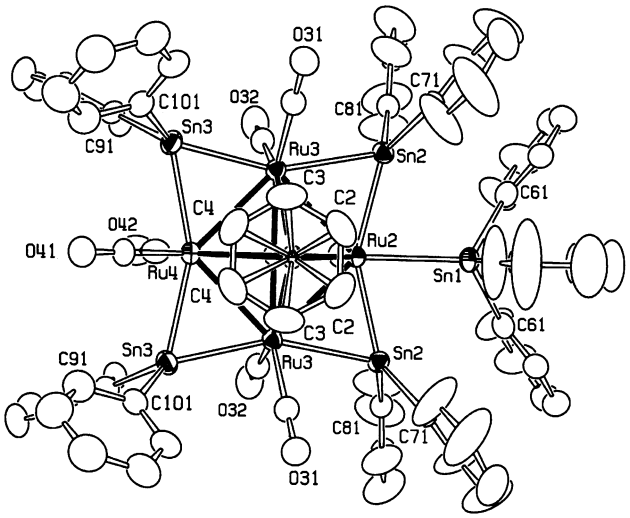

Figure 6. ORTEP diagram of the molecular structure of $Ru_5(CO)_7(SnPh_3)(C_6H_6)(\mu\text{-}SnPh_2)_4(\mu_5\text{-}C)(\mu\text{-}H)$, **8**, showing 40% thermal ellipsoid probability.

Table 9. Selected Intramolecular Distances and Angles for $Ru_5(CO)_7(\mu\text{-}SnPh_2)_4(SnPh_3)(C_6H_6)(\mu_5\text{-}C)(\mu\text{-}H)$, **8**[a]

Distances

atom	atom	distance (Å)	atom	atom	distance (Å)
Ru(1)	Ru(2)	2.9290(11)	Ru(3)	Sn(3)	2.6125(8)
Ru(1)	Ru(3)	2.8208(8)	Ru(4)	Sn(3)	2.6715(6)
Ru(1)	Ru(4)	2.8517(11)	Ru(1)	C(1)	2.065(9)
Ru(2)	Ru(3)	2.9117(8)	Ru(2)	C(1)	2.037(9)
Ru(3)	Ru(4)	2.8670(8)	Ru(3)	C(1)	2.0519(8)
Ru(2)	Sn(1)	2.7559(10)	Ru(4)	C(1)	2.033(9)
Ru(2)	Sn(2)	2.6198(5)	C	O(av)	1.14(1)
Ru(3)	Sn(2)	2.7106(8)			

Angles

atom	atom	atom	angle (deg)	atom	atom	atom	angle (deg)
Ru(1)	Ru(2)	Ru(3)	57.756(19)	Ru(3)	Ru(2)	Sn(1)	132.873(18)
Ru(2)	Ru(3)	Ru(4)	89.54(2)	Ru(2)	Sn(2)	Ru(3)	66.20(2)
Ru(2)	Ru(1)	Ru(4)	89.50(3)	Ru(3)	Sn(3)	Ru(4)	65.71(2)
Ru(1)	Ru(2)	Sn(1)	121.80(4)	Ru	C	O(av)	178(1)

[a] Estimated standard deviations in the least significant figure are given in parentheses.

listed in Table 9. As in compound **4**, compound **8** has also incorporated five tin ligands into the square pyramidal Ru_5

cluster. Four of these tin ligands are bridging $SnPh_2$ groups on each edge of the square base. As in **4**, the fifth tin grouping is a $SnPh_3$ ligand that is terminally coordinated to the basal ruthenium atom, Ru(2), and the Ru−Sn bond distance to this ligand is again long, Ru(2)−Sn(1) = 2.7559(10) Å, as in **4**, 2.7270(11) Å. The Ru−Sn distances to the bridging $SnPh_2$ groups are shorter, range 2.6125(8)−2.7106(8) Å, and similar to those in **4**. Compound **8** contains one bridging hydride ligand (not located directly), δ = −25.63 ppm in the ^{1}H NMR spectrum, that is believed to bridge the long Ru−Ru bond, Ru(1)−Ru(2) 2.9290(11) Å, proximate to the $SnPh_3$ group.

From the reactions affording compounds **3**, **5**, and **6**, we have shown that triphenylstannane can oxidatively add to pentaruthenium carbido carbonyl clusters by reaction of its Sn−H bond to yield stannylpentaruthenium hydride cluster complexes. This would be the first step in the formation of compounds **4**, **7**, and **8**. Indeed, compounds **4** and **8** contain both $SnPh_3$ and hydride ligands. The formation of the $SnPh_2$ groups then occurs by cleavage of a Ph group from an intermediate containing a $SnPh_3$ group. The phenyl group was then combined with the hydride ligand and eliminated as C_6H_6. This is supported by the observation of C_6H_6 formation (by ^{1}H NMR) in the reaction leading to **7** and **8**. Cleavage of phenyl groups from PPh_3 ligands in metal clusters is a well-established transformation.[24] Triruthenium compounds containing multiple SnR_2 bridging groups have been obtained by the reaction of $Ru_3(CO)_{12}$ with SnR_2 precursors;[25] however, the formation of the $SnPh_2$ groups by this route is new, and introduction of four such groups is unique. Interestingly, when treated with CO under pressure (45 atm), compound **8** is converted to **4** by replacement of the benzene ligand with 3 CO ligands, see Scheme 1.

To investigate this tin−phenyl cleavage process still further, we heated compound **5** to 68 °C for 45 min. This treatment yielded the new compound $Ru_5(CO)_{11}(C_6H_6)(\mu_4$-(SnPh)$(\mu_3$-CPh), **9**, in 68% yield. Compound **9** was also characterized crystallographically, and an ORTEP diagram of its molecular structure is shown in Figure 7. Selected bond distances and angles are listed in Table 10. Compound **9** contains the usual square pyramidal cluster of five ruthenium atoms but also has a novel quadruply bridging SnPh (stannylyne group) capping the base of this square pyramid. The Ru−Sn(1) bond distances range 2.6006(13)−2.6836(12) Å. The original benzene ligand is coordinated to ruthenium Ru(1), in the base of the Ru_5 square pyramid. Surprisingly, compound **9** does not contain an interstitial carbido atom but instead contains a benzylidyne ligand, CPh, that bridges the three ruthenium atoms Ru(1), Ru(2), and Ru(5), see eq 3. The Ru−C(1) bond distances to the benzylidyne group range 1.958(11)−2.178(13) Å. We believe that the benzylidene ligand was formed by transfer of a phenyl group from the tin atom to the carbido carbon atom, and the new group then moved out from the interior of the cluster to its surface where it is observed in **9**. In the formation of **9**, two phenyl groups were cleaved from the tin atom. One of the phenyl groups was eliminated from the compound as benzene by combination with the hydride ligand in **5**.

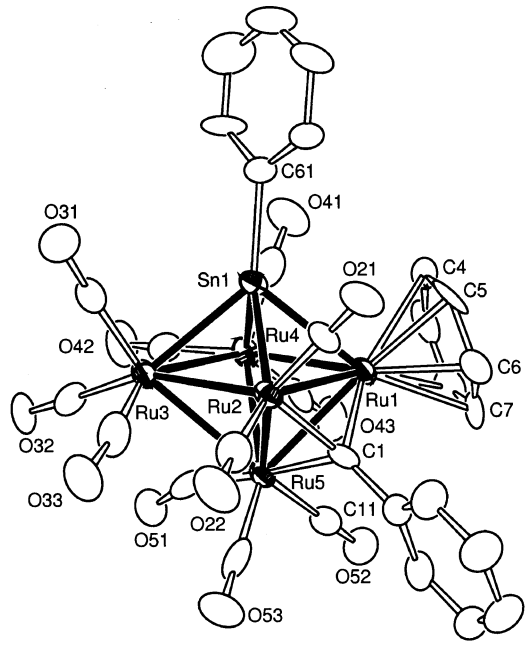

Figure 7. ORTEP diagram of the molecular structure of $Ru_5(CO)_{11}(C_6H_6)$-$(\mu_4$-SnPh$)(\mu_3$-CPh), **9**, showing 40% thermal ellipsoid probability.

Table 10. Selected Intramolecular Distances and Angles for $Ru_5(CO)_{11}(C_6H_6)(\mu_3$-CPh$)(\mu_4$-SnPh), **9**[a]

Distances

atom	atom	distance (Å)	atom	atom	distance (Å)
Ru(1)	Ru(2)	2.7965(13)	Ru(1)	Sn(1)	2.6836(12)
Ru(1)	Ru(4)	2.8958(15)	Ru(2)	Sn(1)	2.6006(13)
Ru(1)	Ru(5)	2.7381(13)	Ru(3)	Sn(1)	2.6453(13)
Ru(2)	Ru(3)	2.8725(15)	Ru(4)	Sn(1)	2.6711(14)
Ru(2)	Ru(5)	2.7941(14)	Ru(1)	C(1)	2.078(11)
Ru(3)	Ru(4)	2.9456(13)	Ru(2)	C(1)	1.958(11)
Ru(3)	Ru(5)	2.9619(13)	Ru(5)	C(1)	2.178(13)
Ru(4)	Ru(5)	2.8090(14)	C	O(av)	1.14(1)

Angles

atom	atom	atom	angle (deg)	atom	atom	atom	angle (deg)
Ru(2)	Ru(1)	Ru(4)	89.74(4)	Ru(2)	Sn(1)	Ru(4)	99.26(4)
Ru(1)	Ru(2)	Ru(3)	93.23(4)	Ru(1)	C(1)	Ru(5)	80.1(4)
Ru(2)	Ru(3)	Ru(4)	87.31(4)	Ru(1)	C(1)	Ru(2)	87.7(5)
Ru(3)	Ru(4)	Ru(1)	89.71(4)	C(11)	C(1)	Ru(1)	128.6(8)
Ru(1)	Sn(1)	Ru(3)	101.28(4)	Ru	C	O(av)	175(1)

[a] Estimated standard deviations in the least significant figure are given in parentheses.

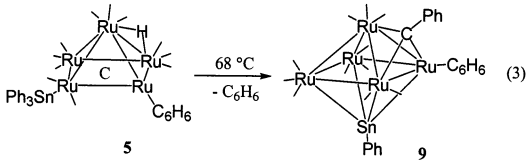

(3)

Benzene formation was confirmed spectroscopically by performing the reaction in an NMR tube. At this point, a

(24) (a) Garrou, P. E. *Chem. Rev.* **1985**, *85*, 171. (b) Bender, R.; Braunstein, P.; Dedieu, A.; Ellis, P. D.; Huggins, B.; Harvey, P. D.; Sappa, E.; Tiripicchio, A. *Inorg. Chem.* **1996**, *35*, 1223.

(25) (a) Cardin, C. J.; Cardin, D. J.; Convert, M. A.; Dauter, Z.; Fenske, D.; Devereux, M. M.; Power, M. B. *J. Chem. Soc., Dalton Trans.* **1996**, 1131. (b) Somerville, D. M.; Shapley, J. R. *Catal. Lett.* **1998**, *52*, 123.

$SnPh_2$ ligand should exist in some intermediate that we did not observe. A second phenyl was then readily cleaved from that tin ligand and shifted to the carbido carbon atom which then moved out from the interior of the cluster to a triply bridging position in the form of the benzylidyne ligand. The resultant tin ligand containing only one Ph group then assumed the quadruply bridging position across the base of the Ru_5 square pyramid to form the stannylyne group. Stannylyne groups are very rare. Curiously, there have been no previous structural characterizations of compounds that contain SnR groups bridging four or even three transition metal atoms. There was, however, one report of a nickel complex, $[Ni_{11}(CO)_{18}(\mu_5\text{-SnMe})_2]^{2-}$, that contained two SnMe groups with each one bridging *five* nickel atoms.[26]

Summary

The facile reactions of pentaruthenium carbonyl reagents with triphenylstannane has yielded new ruthenium−tin clusters complexes with a wide range of Ru/Sn compositions. Complexes containing as many as five tin ligands have been produced. Cleavage of phenyl groups from the tin ligands resulted in the formation of bridging $SnPh_2$ ligands and in one case a novel quadruply bridging SnPh ligand. It is anticipated that these compounds will serve as precursors to new ruthenium−tin nanoclusters that could find useful applications in heterogeneous catalysis.[10]

Acknowledgment. These studies were supported by the Division of Chemical Sciences of the Office of Basic Energy Sciences of the U.S. Department of Energy and the USC Nanocenter.

Supporting Information Available: X-ray crystallographic data in CIF format for compounds **3**−**9** and details of their solution and refinement. This material is available free of charge via the Internet at http://pubs.acs.org.

IC0204169

(26) Zebrowski, J. P.; Hayashi, R. K.; Dahl, L. F. *J. Am. Chem. Soc.* **1993**, *115*, 1142.